J Mater Sci (2008) 43:5023–5027
DOI 10.1007/s10853-008-2742-7

LETTER

Grain size control by pressure application regime during spark plasma sintering of Nd-YAG nanopowders

Rachman Chaim · Zhijian Shen

Received: 26 March 2008 / Accepted: 16 May 2008 / Published online: 1 June 2008
© Springer Science+Business Media, LLC 2008

Recently, spark plasma sintering (SPS) has successfully been used for fabrication of fully dense and transparent oxides [1–4] and nanocrystalline ceramics [5–8]. It was both experimentally [9] and theoretically [10, 11] shown that application of high pressures in SPS may enhance the densification rate at lower temperatures, and hence preserve the nano gain size character of the dense ceramic. Nevertheless, grain growth was found to be an inevitable process in SPS, especially at the final stages of sintering/densification. The driving force for grain growth in pure materials is the grain boundary (gb) curvature [12]. More homogeneous particle size and shape are expected to decrease this driving force. Therefore, control of the nanostructure green compact prior to and during the SPS process via the processing parameters may be beneficial for controlling the final grain size. In the present work, we examined the effect of the pressure application regime on densification and final grain size during the SPS of neodymium-doped yttrium aluminum garnet (Nd-YAG) nanocrystalline powder compacts.

Commercial nanocrystalline powders of YAG doped with 2 mol% Nd (NanoAmor Inc., TX, USA) and 99.5% purity were used. The main impurity contents according to the manufacturer were (in ppm): 70 Eu, 60 La, 30 Ce, 30 Gd, 20 Sm, 8 Si, 3 Cu, Pb, and Zn, 2 Fe and Ni. The powder nanoparticles (40 nm average particle diameter) were softly agglomerated. Analysis of the nano-powder by X-ray diffraction exhibited a few wide peaks that fit those of orthorhombic $Al_2Y_4O_9$ composition (JCPDS# 14-475). Disc shape specimens with final dimensions of 12 mm in diameter and 2 mm thick were fabricated using Dr. Sinter 2050 (Sumitomo Coal Mining Co. Ltd., Japan) located at Stockholm University. The nanocrystalline powder was poured into the graphite die and pre-pressed to 100 MPa before heating. The compact powder was shielded from the graphite die and punch surfaces using graphite foils. The 100 MPa pressure was applied by two different regimes either at 1,200 °C (designated as T12) or at the SPS temperature (herein designated as TS). The SPS duration was 5 min at the SPS temperature. Finally, the load was released and the specimen was cooled to the room temperature. The heating rate 100 °C/min was used. The grain size was measured from the polished and thermally etched surfaces using high-resolution scanning electron microscope (HRSEM, Leo Gemini 982). The larger axes of the grains were directly measured for each specimen, using at least 400 grains for the particle size statistics. The relative density of the sintered specimens was measured by the Archimedes technique using the water media and the value of 4.5770 g cm^{-3} as the theoretical density of the Nd-doped YAG.

The relative density of the sintered specimens for both pressure application regimes exhibited very similar behavior versus the SPS temperature (Fig. 1a). The density of the specimen pressed via T12 at the lowest SPS temperature (i.e., 1,300 °C) was lower by a few percent than the TS regime. Nevertheless, all the specimens at higher temperatures reached comparable densities around 98–99%, regardless of the pressure application regime. On the other hand, significantly different behavior was observed in the corresponding grain size evolution of the T12 and TS regimes versus the SPS temperature (Fig. 1b). In this

R. Chaim (✉)
Department of Materials Engineering, Technion-Israel Institute of Technology, Haifa 32000, Israel
e-mail: rchaim@technion.ac.il

Z. Shen
Department of Inorganic Chemistry, Arrhenius Laboratory, Stockholm University, 106 91 Stockholm, Sweden

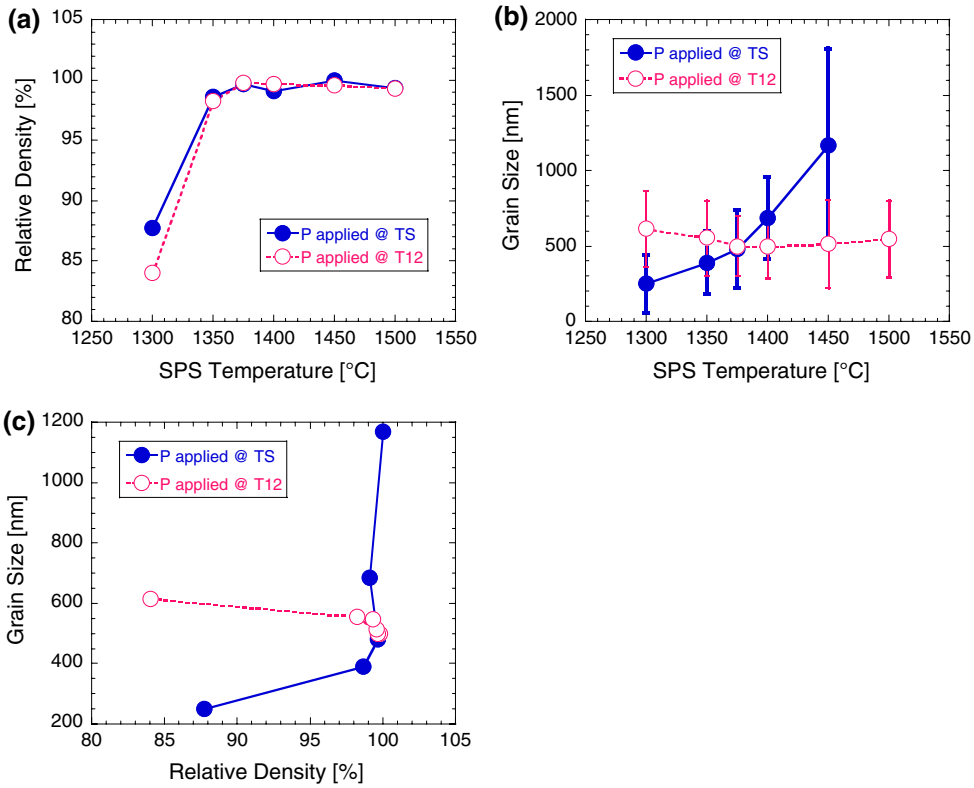

Fig. 1 (**a**) Relative density versus temperature, (**b**) grain size versus temperature, and (**c**) grain size versus relative density dependencies in the Nd-YAG after SPS for 5 min at 100 MPa

respect, the TS regime resulted in continuous increase in the average (mean) grain size with the SPS temperature, from 250 nm at 1,300 °C to 1,170 nm at 1,450 °C. In contrast, the grain size in the T12 regime was almost constant between 500 and 600 nm over the entire SPS temperature range. The standard deviations of the grain size data shown in Fig. 1b confirmed this trend. The corresponding grain size–relative density trajectory for the two pressure application regimes were shown in Fig. 1c and exhibit the suppressing effect of the T12 regime on the grain growth. This surprising result where the final grain size in the nanometer range may be controlled via the pressure application regime will be discussed below in conjunction with evolution of the particles and their coarsening. In all cases, the sintered specimens exhibited the cubic symmetry of the stoichiometric YAG, $Y_3Al_5O_{12}$ (JCPDS# 33-0040) in the X-ray diffraction spectra (not shown here). The present specimens were transluscent to opaque compared to the previously fabricated transparent YAG specimens [3]. This may arise from the relatively low purity of the original powder (99.5%).

The sintered microstructures at different SPS temperatures were characterized for both regimes and exhibited distinctly different character. Sub-micrometer size grains with almost spherical morphology and narrow size distribution (615 ± 250 nm) were observed in the partially dense specimen sintered at 1,300 °C under T12 condition (Fig. 2a). This was followed by dense specimens at higher temperatures (Fig. 2b, c) where the equiaxed nature of the grains and their narrow size distribution were preserved (Fig. 3d). In addition, the majority of the grain boundaries cross sections (observed in 2D) revealed planar nature (Fig. 2c) with triple junction angles tending to the equilibrium dihedral angle of 120°. It should be emphasized that the lack of curvature at such planar grain boundaries lowers the driving force for grain boundary migration, hence suppresses the grain growth. In comparison, the microstructure of the specimens sintered at the similar SPS temperatures but under the TS pressure application regime exhibited different characteristics (Fig. 3). In the partially dense specimen at 1,300 °C, albeit sub-micrometer in size, the grain size distribution was significantly widened and exhibited a bimodal character; large number of smaller grains (250 ± 190 nm) and small number of larger grains (1,265 ± 300 nm) were present (Fig. 3d). This bimodal grain size distribution was consistent also at 1,350 °C (i.e., 390 ± 210 nm smaller grains versus 1,800 ± 470 nm larger grains). The volume distribution of the grains revealed that the grains smaller than 390 nm occupied a negligible fraction (<1%) of the specimen volume only. However, at higher SPS temperatures the smaller grains disappeared while the larger grains persisted (Fig. 3b, c).

Analysis of the mean grain size from the TS regime with respect to the grain growth kinetic equation [13] resulted in an Arrhenius plot with activation energy 525 ± 14 kJ mol^{-1} and the grain growth exponent $n = 2$ as shown in Fig. 4. This

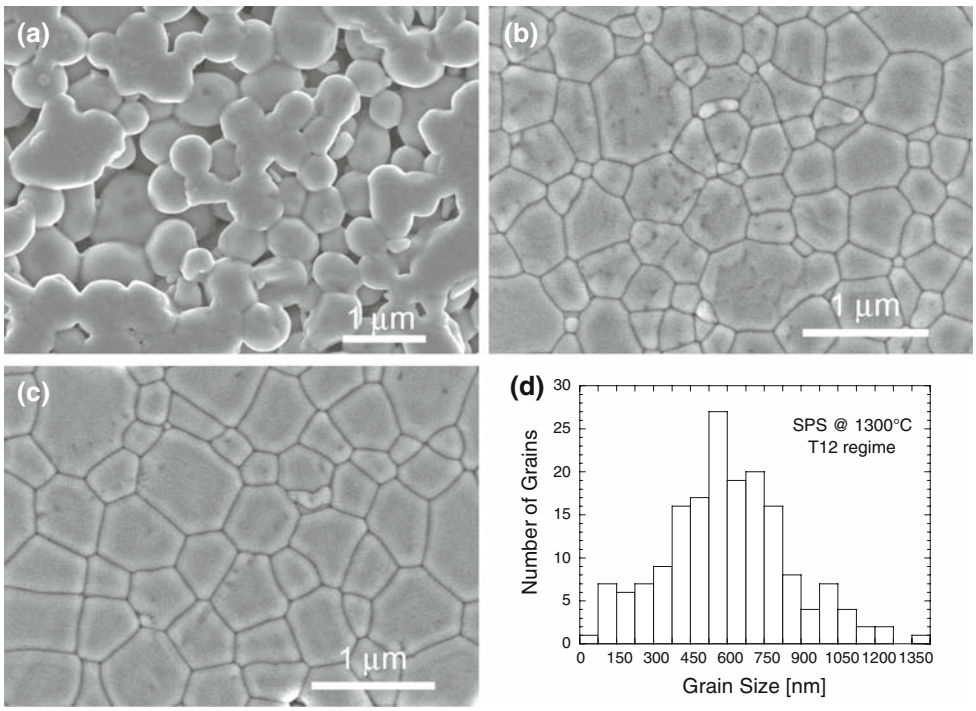

Fig. 2 HRSEM images from the Nd-YAG specimens after SPS for 5 min and 100 MPa at (**a**) 1,300 °C, (**b**) 1,400 °C, and (**c**) 1,500 °C. (**d**) The grain size distribution for the image in (**a**) exhibits mean grain size 615 ± 250 nm at 1,300 °C. The pressure was applied at 1,200 °C (T12 regime)

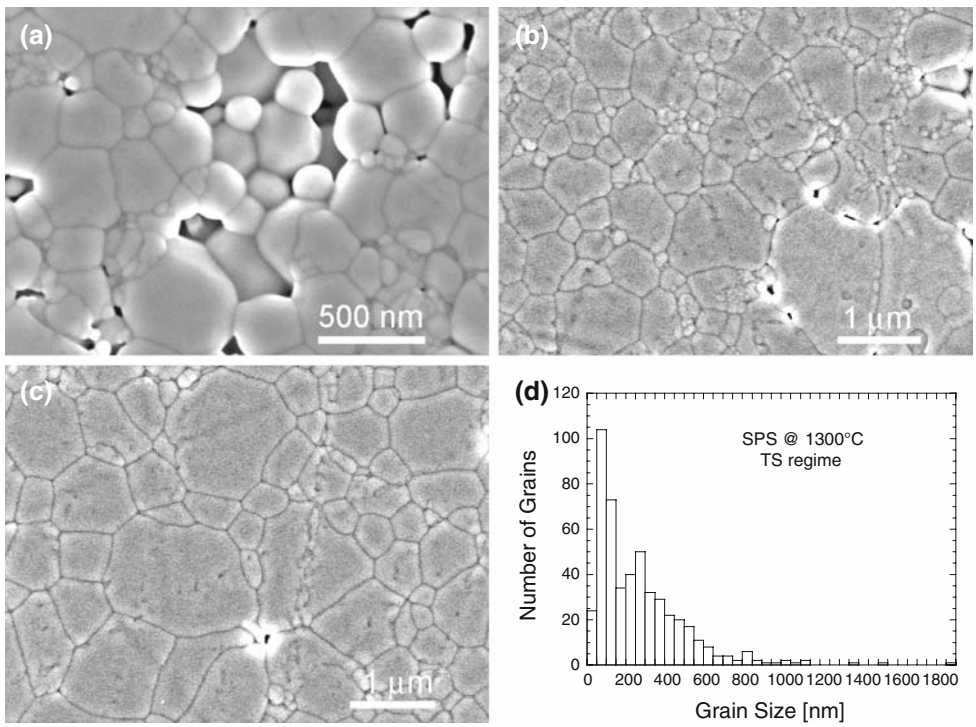

Fig. 3 HRSEM images from the Nd-YAG specimens after SPS for 5 min and 100 MPa at (**a**) 1,300 °C, (**b**) 1,400 °C, and (**c**) 1,450 °C. (**d**) The grain size distribution for the image in (**a**) exhibits two mean grain sizes 250 ± 190 nm and 1,265 ± 300 at 1,300 °C. The pressure was applied at the SPS temperatures (TS regime)

activation energy is close to the activation energy (540 kJ mol^{-1}) reported for grain growth in dense YAG fibers between 1,400 and 1,700 °C [14] and 553 kJ mol^{-1} in YAG specimens formed by SPS [15] and confirmed the normal grain growth for the TS regime.

It should be noted that neither YAG nor Nd-YAG is expected to undergo plastic deformation under the temperature–pressure regimes used in the present study. This is due to the very high yield stresses of YAG at high temperatures as reviewed earlier [16]. The yield stress of YAG single crystal at 1,800 °C was estimated about 380 MPa in support to its very high creep resistant behavior [17]. Consequently, the densification of the present specimens cannot be accounted for plastic deformation via

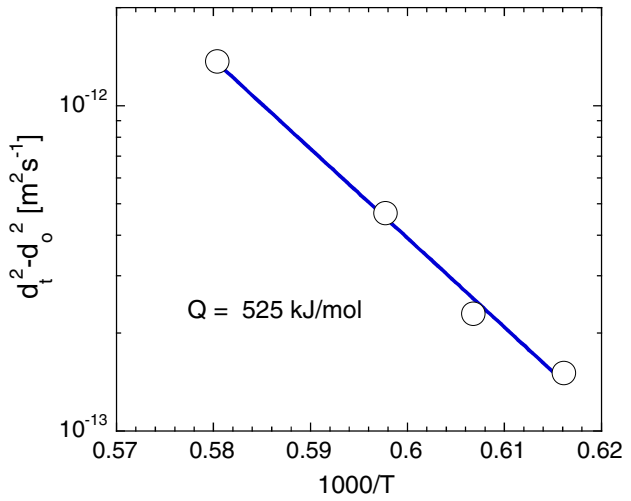

Fig. 4 Arrhenius plot showing the activation energy of 525 ± 14 (kJ mol^{-1}) for the grain growth exponent $n = 2$ as normal grain growth (TS regime data)

dislocation slip within the bulk of the nanoparticle crystallites. Alternatively, previous analysis of the densification mechanisms and microstructural evolution of YAG during SPS below 1,400 °C was consistent with grain sliding and rotation, aided by viscous layer, due to softening of the nanoparticle surfaces by the plasma [3]. This mechanism was dominating at lower densities where free surfaces at open pores are available for the plasma activation. However, above 1,400 °C and at higher densities (i.e., >90%) where pores become isolated, this mechanism is no more active, and curvature-driven grain growth takes place. Therefore, the effect of the pressure application regime in the present study can be understood with respect to the evolving microstructure during the SPS.

Based on the observed microstructure, significant nanoparticle coarsening occurs during the heating stage, prior to the pressure application. Particle coarsening is accelerated with the temperature increase as well as the electric field effects. However, it was found that application of pressure already at lower temperatures (i.e., T12 regime) lead also to narrower particle size distribution of the coarsened particles.

The final grain size is determined by two consecutive processes: particle coarsening in porous compact, followed by grain growth in the denser state. It is reasonable to assume that surface diffusion processes, in the porous Nd-YAG compact, become significant at temperatures above ~600 °C (0.4 T_m), where T_m is the melting temperature of YAG (2,243 K). Particle coarsening may follow the kinetic law with particle size exponents $n = 3$ (diffusion through liquid layer, evaporation–condensation) or $n = 4$ (surface diffusion), compared to $n = 2$ (grain boundary diffusion) for normal grain growth in dense compacts [13]. Therefore, higher growth rate is expected during the coarsening compared to the normal grain growth. Since both coarsening and grain growth are curvature driven, the former will result in wider particle size distribution than does normal grain growth. Consequently, the longer the coarsening duration and the higher its temperature (prior to pressure application), the wider becomes the particle/grain size distribution, in agreement with the experimental results.

Application of pressure at lower temperatures (i.e., T12 regime) should result in homogeneous compaction of the coarsened nanoparticles, with narrow size distribution, due to the more homogeneous distribution of the applied stress at the particle contact points; densification will proceed by grains sliding over each other. This may result in densification and planar grain boundaries where the diffusional processes are restricted to the grain boundary regions. It should be noted that once dense compact forms under the pressure, the pressure ceases to affect the grain boundary curvature. Further growth of such microstructure should be suppressed due to lack of grain boundary curvature which acts as a driving force for the grain growth.

On the other hand, application of the pressure at higher SPS temperatures (i.e., TS regime) enables significant coarsening of the nanoparticles during the heating up that may result in bimodal particle/grain size distribution. Such microstructure will also experience pressure-assisted densification via particle surface processes. Nevertheless, the wider particle size distribution, due to extended coarsening effect, is expected to result in non-homogeneous distribution of the applied stress at the particle contact points. Consequently, curved, non-planar grain boundaries may result in the dense compact, prone to curvature-driven normal grain growth, in the dense state, as was observed.

The present experimental results point to several important aspect during the SPS of nanocrystalline powders. Particle coarsening during the heating up may have strong impact on the final grain growth behavior and cannot be neglected. Particle coarsening during the heating may vary the particle size distribution, depending on the coarsening mechanism. This, in turn, affects the grain boundary curvature immediate to pressure application. Therefore, application of the SPS pressure before significant coarsening of the nanoparticles should be beneficial for suppressing further grain growth in the dense compact.

Acknowledgement The support of the Israel Ministry of Defense and the Fund for Promotion of Research at the Technion and the Swedish Research Council through grant 621-2005-6299 are gratefully acknowledged.

References

1. Chaim R, Shen Z, Nygren M (2004) J Mater Res 19:2527. doi: 10.1557/JMR.2004.0334

2. Kim BN, Hiraga K, Morita K, Yoshida H (2007) Scr Mater 57:607. doi:10.1016/j.scriptamat.2007.06.009
3. Chaim R, Marder-Jaekel R, Shen JZ (2006) Mater Sci Eng A 429:74. doi:10.1016/j.msea.2006.04.072
4. Jiang D, Hilbert DM, Kuntz JD, Anselmi-Tamburini U, Mukherjee AK (2007) Mater Sci Eng A 463:89
5. Nygren M, Shen Z (2003) Solid State Sci 5:125. doi:10.1016/S1293-2558(02)00086-9
6. Mishra RS, Risbud SH, Mukherjee AK (1998) J Mater Res 13:86. doi:10.1557/JMR.1998.0013
7. Li W, Gao L (2000) J Eur Ceram Soc 20:2441. doi:10.1016/S0955-2219(00)00152-7
8. Wang L, Jiang W, Chen L (2004) J Mater Sci 39:4515. doi:10.1023/B:JMSC.0000034145.54280.53
9. Anselmi-Tamburini U, Garay JE, Munir ZA (2006) Scr Mater 54:823. doi:10.1016/j.scriptamat.2005.11.015
10. Munir ZA, Anselmi-Tamburini U, Ohyanagi M (2006) J Mater Sci 41:763. doi:10.1007/s10853-006-6555-2
11. Chaim R, Margulis M (2005) Mater Sci Eng A 407:180. doi:10.1016/j.msea.2005.07.024
12. Kang SJL (2005) Sintering densification grain growth & microstructure. Elsevier, Oxford
13. Rahaman MN (2007) Ceramic processing. CRC Press, Boca Raton
14. King BH, Halloran JW (1995) J Am Ceram Soc 78:2141. doi:10.1111/j.1151-2916.1995.tb08626.x
15. Chaim R (2006) J Mater Sci 41:7862. doi:10.1007/s10853-006-0605-7
16. Chaim R (2007) Mater Sci Eng A 443:25. doi:10.1016/j.msea.2006.07.092
17. Blumenthal WR, Philips DS (1996) J Am Ceram Soc 79:1047. doi:10.1111/j.1151-2916.1996.tb08546.x